There is experimental evidence in favor of this suggestion. Figure 4 presents spectra of polariton emission recorded at high angular resolution and high density of resonant excitation. In the range $k < 0$, the signal is seen to decrease as $|k|$ rises. But the behavior changes at $0 < k < k_{ex}$, when intense two-photon scattering is accompanied by a sharp narrowing of the line observed at $k = 0$, $2k_{ex}$, and near $k = k_{ex}$.

So far we have investigated the behavior of polaritons excited by circularly polarized light. Note, however, that the energy $2\hbar\omega(k_{ex})$ is close (lower by 1–2 meV) to the ground energy of the biexciton state in the quantum well. The state is spin singlet and optically active for two-photon scattering of linearly polarized light. Under excitation by elliptically polarized light its optical activity decreases gradually down to zero as the degree ρ_{ex} of circular polarization of exciting light varies from 0 to 1. Thus, the two-photon scattering is expected to be resonant and to increase sharply at linearly polarized light.

Figure 5 presents the dependences ρ_{LP} and $I_{LP} = I_{LP^+} + I_{LP^-}$ on ρ_{ex} at two different densities of excitations. As is seen, I_{LP} increases when the circularly polarized light is replaced by the linearly polarized one. The effects become more pronounced as the density of excitation increases. At $P = 540$ W cm^{-2} I_{LP} increases by several times, growing mainly at $\rho_{ex} < 0.6$. Under the conditions of spontaneous two-photon scattering, the degree of circular polarization of the LP line should disappear monotonically with decreasing ρ_{ex}. Conversely, at high excitation density of excitations ρ_{LP} grows considerably as ρ_{ex} decreases and at $\rho_{ex} \sim 0.6$ even exceeds the polarization degree of exciting light. Only at $\rho_{ex} < 0.4$ the value of ρ_{LP} decreases rapidly down to zero. The behavior of the circular polarization of the LP line is an additional evidence that the two-photon scattering process is excited by elliptically polarized light and that the process is stimulated.

Thus, studying the angle-resolved emission spectra of MC with quantum wells in a wide range of densities of the excitation we have found the conditions at which polaritons with high filling factors are excited at the LPB bottom. Under these conditions we observed and studied strong nonlinear effects in intensity and polarization degree of polariton emission, and demonstrated that these nonlinearities occur in the strong coupling regime.

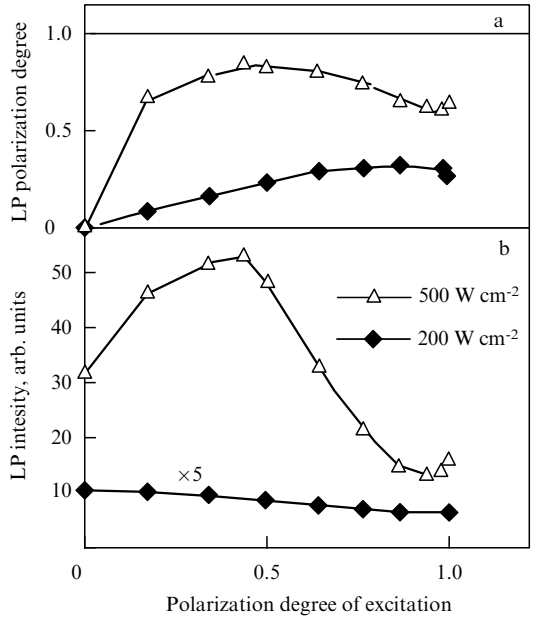

Figure 5. Dependencies of degree of circular polarization ρ_{LP} (a) and intensity of the LP line $I_{LP} = I_{LP^+} + I_{LP^-}$ (b) on the degree of circular polarization of the excitation at $P = 200$ and 540 W cm^{-2}.

In conclusion, we wish to thank M Bayer, L V Butov, N A Gippius, L V Keldysh, V B Timofeev, and S G Tikhodeev for fruitful discussions. The work was supported by the RFBR (Grant 00-02-17120) and Program "Nanostructures".

References

1. Weisbush C et al. *Phys. Rev. Lett.* **69** 3314 (1992)
2. Skolnick M S, Fisher T A, Whittaker D M *Semicond. Sci. Technol.* **13** 645 (1998)
3. Khitrova G et al. *Rev. Mod. Phys.* **71** 1591 (1999)
4. Whittaker D M et al. *Phys. Rev. Lett.* **77** 4792 (1996); Savona V et al. *Phys. Rev. Lett.* **78** 4470 (1997)
5. Houdre R et al. *Phys. Rev. Lett.* **73** 2043 (1994)
6. Imamoglu A et al. *Phys. Rev. A* **53** 4250 (1996)
7. Pau S et al. *Phys. Rev. A* **54** R1789 (1996)
8. Dang Le Si et al. *Phys. Rev. Lett.* **81** 3920 (1998)
9. Tassone F et al. *Phys. Rev. B* **56** 7554 (1997)
10. Tartakovskiĭ A I et al. *Phys. Rev. B* **60** R11293 (1999)
11. Tartakovskiĭ A I et al. *Phys. Rev. B* R2283 (2000)
12. Krizhanovskiĭ D N et al. *Solid State Commun.* (2001) (in press)
13. Tassone F et al. *Phys. Rev. B* **53** R7642 (1996)
14. Honerlage B, Bivas A, Phach Vu Duy *Phys. Rev. Lett.* **41** 49 (1978)
15. The scheme is only qualitative. Renormalization of polariton states, caused by polariton–polariton interactions should be taken into account for precise calculations

Spectroscopy of electron–electron scattering in a 2DEG

H Buhmann, H Predel, L W Molenkamp, R N Gurzhi, A N Kalinenko, A I Kopeliovich, A V Yanovsky

Abstract. Experimentally electron-beam injection and detection via quantum point-contacts is used to investigate the scattering of a non-equilibrium electron distribution in a two-dimensional electron gas (2DEG) of a GaAs/(Ga,Al)As heterostructure. The energy dependence of electron–electron scattering processes has been studied in a weak magnetic field by investigating the detector signal. Assuming electron beams with a narrow opening angle a magnetic field B perpendicular to the 2DEG plane causes only electrons which are scattered in a point O at an angle α to reach the detector. Thus, it is possible to measure directly the energy dependence of the angular electron distribution after scattering. The experimental data give a clear evidence for the importance of small angle scattering processes in two-dimensional systems, as predicted theoretically.

H Buhmann, H Predel, L W Molenkamp Physikalisches Institut, Universität Würzburg, Am Hubland, D-97047 Würzburg, Germany
R N Gurzhi, A N Kalinenko, A I Kopeliovich, A V Yanovsky B I Verkin Institute for Low Temperature Physics and Engineering, National Academy of Sciences of Ukraine, Lenin Ave. 47, 31064 Khar'kov, Ukraine

The scattering characteristics of electrons in systems with reduced dimensions are expected to exhibit decisive differences with respect to three-dimensional (3D) systems. Theoretically, electron–electron (ee) scattering in two-dimensional (2D) systems was first considered in the early seventies [1]. Further numerical evaluations followed in the early eighties [2]. It was shown that the lifetime of a non-equilibrium electron in a 2DEG is shorter by a factor of order $\ln(\varepsilon_F/\varepsilon)$ compared to the 3D case (ε is the electron's excess energy counted from the Fermi energy, ε_F).

A reduction of the dimensionality induces much more drastic changes in the momentum transfer processes [3–7]. Two types of ee-collisions with nearly the same probability characterize scattering in 2D systems [3]. First, collisions of a non-equilibrium electron with momentum $\mathbf{p}$ and excess energy ε with equilibrium electrons of momentum $\mathbf{p}_1$ usually result in scattering of both electrons by a small angle $\alpha \sim \varepsilon/\varepsilon_F$ into states $\mathbf{p}_2$ and $\mathbf{p}_3$ leaving a hole (an empty place in Fermi distribution) in the state $\mathbf{p}_1$, with $\mathbf{p} + \mathbf{p}_1 = \mathbf{p}_2 + \mathbf{p}_3$. Second, collisions with electrons of nearly opposite momentum, $\mathbf{p} \approx -\mathbf{p}_1$. In this case, the electrons at $\mathbf{p}_2$ and $\mathbf{p}_3 \approx -\mathbf{p}_2$ are scattered by a much larger arbitrary angle, on average $\alpha \approx \sqrt{\varepsilon/\varepsilon_F}$.

Up to now no direct experimental evidence for these 2D effects in ee-scattering has been demonstrated. Recently, we studied experimentally and theoretically the influence of electron–electron collisions on the propagation of electron beams in a 2DEG for excess injection energies ranging from zero up to the Fermi energy [8]. We found that the detector signal consists of *quasiballistic* electrons, which either have not undergone any electron–electron collisions or have only been scattered at small angles. Theoretically, the small-angle scattering exhibits distinct features that can be traced back to the reduced dimensionality of the electron system. A number of nonlinear effects, also related to the two-dimensional character of the system, were discussed. In the simplest situation, the heating of the electron gas by the high-energy part of the beam leads to a weakening of the signal of quasiballistic electrons and to the appearance of thermovoltage. This results in a nonmonotonic dependence of the detector signal on the intensity of the injected beam, as observed experimentally. Extending the experimental techniques used in that paper, we now have been able to extract compelling evidence for the preponderance of small-angle scattering in 2D systems directly.

In the experiment, an electron beam injected into the 2DEG via an electrostatically defined quantum point-contact (QPC_i) is detected by a second (QPC_d) in a certain distance [9, 10], schematically shown in Fig. 1. When a magnetic field is applied perpendicular to the 2DEG plane, the injected beam is deflected and only scattered electrons can reach the detector QPC_d. At low electron excess energies, $\varepsilon \ll \varepsilon_F$, one can neglect the energy dependence of the cyclotron radius r_c. When the opening angle Φ of QPC_i and QPC_d [9] is sufficiently small i.e., $\Phi \ll 1$, we have that for a given magnetic field B the detector signal is determined only by one trajectory i.e., the signal results solely from electrons that were scattered in point O across an angle $\alpha = 2\arcsin(L/2r_c)$ (see Fig. 1). Thus, by changing the magnetic field we can directly measure the angular distribution function of scattered electrons in a wide range of angles α.

As mentioned above, the angular scattering distribution will in general depend on the excess energy ε of the injected electrons. This is why we apply a differential measurement

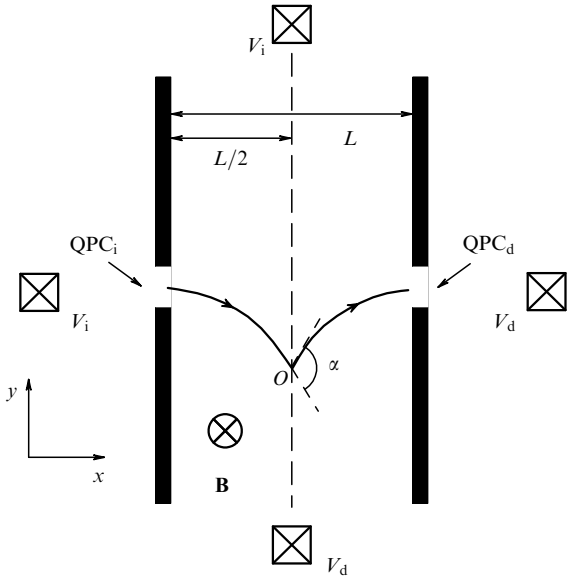

Figure 1. Schematic view of the sample structure showing the Schottky gates (black areas) defining the injector (QPC_i) and detector (QPC_d) quantum point contacts. Also indicated is a possible trajectory of an injected electron in a perpindicular magnetic field B, where the electron is scattered in point O over an angle α. Crossed squares represent the ohmic contacts.

technique, which is equivalent to using mono-energetic electron beams. Energy ε is controlled by adjusting the bias voltage V_i applied between the contacts denoted V_i in Fig. 1. The non-local voltage drop V_d measured between contacts V_d results from electrons that have reached the detector QPC and charge the 2DEG area beyond QPC_d. A small ac modulation $\delta V_i \ll V_i$ is added to the dc bias. Although an electron beam injected via a QPC consists of electrons of all energies from ε_F up to $\varepsilon_F + \varepsilon$, only the contribution δV_d of the high-energy part of the beam to the signal can be detected by measuring the signal with a lock-in at the same frequency as δV_i.

For the experiments, conventional Si-modulation doped GaAs/(Ga,Al)As heterosturctures were used, with a carrier concentration of $n_s \simeq 2.8 \times 10^{11}$ cm^{-2} and an electron mobility of $\mu \simeq 100$ m^2(Vs)$^{-1}$, which implies an impurity mean free path of $l_{imp} \geq 10$ μm. A pair of QPCs, about $L \approx 4$ μm apart, were fabricated using split-gate technology. By applying a negative voltage to the gate contacts, the conductance of the QPCs ($G_{QPC} = N2e^2/h$) could be adjusted from several conducting modes N into the tunneling regime ($N < 1$). Throughout all experiments injector and detector QPC were adjusted to $N = 1$ to ensure narrow opening angles and ballistically transmitted electrons [9]. The injection dc voltage, V_i, was varied between 0 and 5 mV. The ac modulation voltage was kept constant at 30 μV, so that $\delta V_i \leq k_B T_0/e \ll V_i$. The sample was kept at a lattice temperature $T_0 \approx 200$ mK in a dilution refrigerator.

Figure 2 displays some examples of the measured detector signal for various injection voltages as a function of magnetic field. At low injection energy $eV_i = 0.1$ meV, the ee-scattering mean free path l_{ee} is much larger than L and the electrons reach the detector QPC ballistically. From this we determine the characteristic opening angle [9] of injector and detector, $\Phi \approx 12°$. The detector signal is at maximum at zero magnetic field. With increasing injection energy V_i, ee-scattering becomes more important, leading to (i) a decrease of the

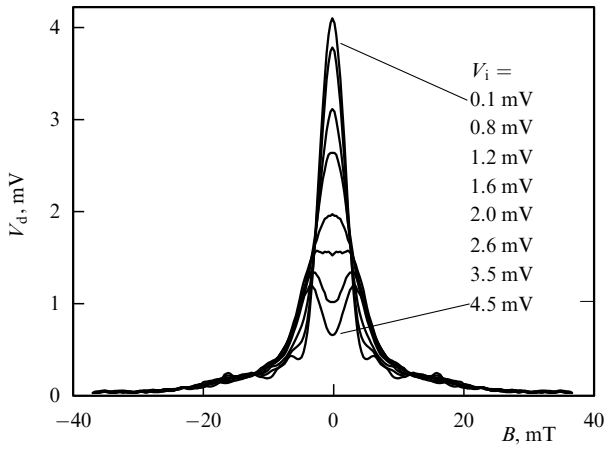

Figure 2. Behavior of the electron beam signal at different injector voltages as a function of magnetic field B.

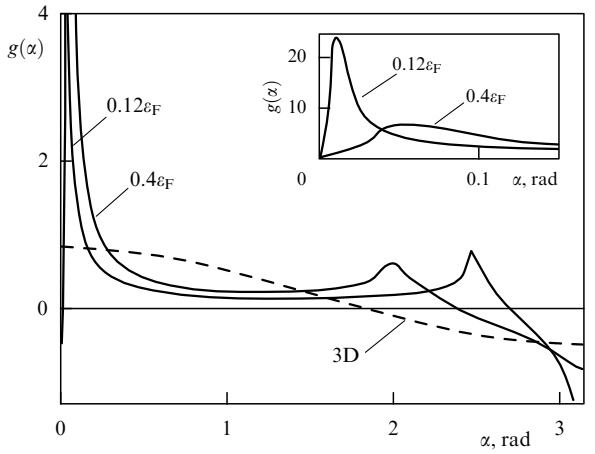

Figure 3. Angular electron–electron scattering distribution function $g(\alpha)$ in a 2D system (solid line) at $T = 0$ for two different injection energies compared with the 3D case (dashed line).

signal of non-scattered electrons near $B = 0$, (ii) a broadening of the signal with B and (iii) the appearance of a dip in the signal around $B = 0$ for energies $V_i \geqslant 3.5$ mV.

For further consideration we have to investigate how this experimental behavior relates quantitatively to the expected 2D-scattering characteristics. Therefore, we describe the problem by a linearized Boltzmann equation in magnetic field:

$$\omega_c \frac{\partial f}{\partial \varphi} + v_x \frac{\partial f}{\partial x} + v_y \frac{\partial f}{\partial y} = \hat{J} f, \tag{1}$$

where ω_c is the cyclotron frequency and $\hat{J}$ is the linearized operator of the ee-collisions, which can be written as

$$\hat{J} f(\mathbf{p}) = -\nu f(\mathbf{p}) + \int \mathrm{d}\mathbf{p}'\, \nu_{\mathbf{p}\mathbf{p}'} f(\mathbf{p}')\,, \tag{2}$$

with $\nu = \int \mathrm{d}\mathbf{p}'\, \nu_{\mathbf{p}'\mathbf{p}}$. Integration of the collision integral kernel $\nu_{\mathbf{p}'\mathbf{p}}$ over energy yields the angular distribution function of the scattered electrons [7]:

$$g(\alpha) = m v^{-1} \int \mathrm{d}\varepsilon'\, \nu_{\mathbf{p}'\mathbf{p}}\,, \tag{3}$$

where α is the angle between $\mathbf{p}$ and $\mathbf{p}'$, and $\mathbf{p}'$ refers to the electrons (holes) at $\mathbf{p}_1$, $\mathbf{p}_2$ and $\mathbf{p}_3$ mentioned above. By definition, $|g(\alpha)|\,\mathrm{d}\alpha$ is the probability that a non-equilibrium electron, $g(\alpha) > 0$ (or hole for $g(\alpha) < 0$), emerges in an interval $\mathrm{d}\alpha$ after scattering. In Figure 3 this function $g(\alpha)$ is shown for two different electron excess energies ε. For comparison, we have also plotted the most commonly used approximation for $g(\alpha)$ for 3D systems, $g(\alpha) \propto 1 + 2\cos(\alpha)$, and independent of ε [11]. For 3D systems $g(\alpha)$ is very smooth, exhibiting a broad distribution of electrons moving in forward direction and holes moving backwards. In the 2D case $g(\alpha)$ shows several distinct features. Most conspicuous is a very narrow distribution of electrons moving in forward direction. The height of this peak is determined by the small-angular processes of the first type; its width is determined by second-type processes and increases with energy according to $\delta\alpha \sim (\varepsilon/\varepsilon_F)^{1/2}$. The second type of scattering events also cause a secondary peak at $\alpha \approx \pi - 2(\varepsilon/\varepsilon_F)^{1/2}$ and a narrow hole dip of width $(\varepsilon/\varepsilon_F)^{1/2}$ at $\alpha = \pi$ [7]. However, these effects occur in the backscattering direction and are quite small, so that they will be difficult to detect experimentally. For a comparison with experiments we therefore focus on angles $\alpha < 1$ (rad), where the small-angular scattering peak should provide a clear token of specific 2D phenomena. Another intriguing feature of $g(\alpha)$, which can be seen more clearly in the inset of Fig. 3, is a dip in forward direction for *very* small angles, with a width $\sim 0.1(\varepsilon/\varepsilon_F)^{3/2}$. This dip is caused by the conservation laws. The electron may give away its surplus energy to equilibrium partners only upon scattering by a finite angle. This effect, which was discussed earlier in Refs [4,12], also occurs in 3D systems. However, in 2D the amplitude of the dip is enhanced by a factor $\varepsilon_F/\varepsilon$.

If the probability for an electron to be scattered over a distance L is small (i.e., $l_{ee}(\varepsilon) = v\nu^{-1} \gg L$), Eqn 1 can be solved using perturbation theory on the collision integral. When we write the electron distribution function at the exit of the injector as $f_0 = \delta V_i\, \delta(\varepsilon - V_i)\, \lambda_F \delta(y) \rho_i(\varphi)$, and consider only the first iteration of the collision integral, we can obtain an expression for the current through the detector QPC. For low injection energies $eV_i = \varepsilon \ll \varepsilon_F$, the detector signal can be written as

$$\begin{aligned}
\delta V_d^s &\approx C\, v \int_{-\pi/2}^{\pi/2} \mathrm{d}\varphi \int_{\varphi_0}^{\varphi} \mathrm{d}\varphi'' \int_{-\pi/2}^{\pi/2} \mathrm{d}\varphi'\, \rho_d(\varphi)\, \rho_i(\varphi_1) \cos\varphi \\
&\quad \times g(\varphi'' - \varphi', V_i) \delta(\cos\varphi + \cos\varphi' - \cos\varphi'' - \cos\varphi_1)\,, \\
\varphi_0 &= \arcsin\left(\sin\varphi - \frac{L}{r_c}\right), \\
\varphi_1 &= \arcsin(\sin\varphi' - \sin\varphi'' + \sin\varphi_0)\,.
\end{aligned} \tag{4}$$

Here $C = 2mL\lambda_F \delta V_i (he)^{-1}$, λ_F is the Fermi wavelength and $\rho_i(\varphi)$ ($\rho_d(\varphi)$) is the angular emittance (acceptance) function of the injector (detector) QPC [9]. From this equation it is clear that $g(\alpha)$ can be obtained from the magnetic field dependence of δV_d^s.

When $g(\alpha)$ varies only slightly on the scale of the opening angle Φ, a local approximation to the integrals in Eqn (4) can be made, yielding

$$\delta V_d^s = 2C\, \nu K(\alpha, \Phi) g(\alpha, V_i), \quad \alpha = 2 \arcsin \frac{L}{2r_c}\,. \tag{5}$$

The factor K is given by $K \approx r_c/L\sqrt{1-(L/r_c)^2}$ for $\Phi < \alpha < \pi - 2\sqrt{\Phi}$, and $K \approx 1/\Phi$ for $\alpha < \Phi$. Note that for small enough beam energies V_i, a local approximation of Eqn (5) is invalid for scattering angles $\alpha \leqslant \Phi$, and Eqn (5) only yields a smoothed (by the emittance and acceptance functions) approximation of $g(\alpha)$. The local approximation is also invalid for large scattering angles, $\pi - \alpha < 2\sqrt{\Phi}$.

However, it is possible to extend the range of validity for this one-collision approximation. This is because in all experiments we have $V_i \gg T$, implying that the probability for secondary ee-collisions is approximately an order of magnitude lower than that of the first one [5, 7, 13]. It turns out that a one-collision approximation is valid as long as $L < l_{ee}(eV_i/3) \approx 10\, l_{ee}(V_i)$, i.e. for a much wider range of parameters than the perturbation theory. Partial summation of the corresponding iteration series of Eqn (1) results in the following expression for $\tilde{g}(\alpha, V_i)$:

$$\tilde{g}(\alpha, V_i) = \exp\left(-\frac{\Lambda}{l_{ee}}\right) g(\alpha, V_i)\,, \tag{6}$$

which replaces $g(\alpha, V_i)$ in Eqns (4), (5). The exponential factor on the r.h.s. gives the probability for an electron to travel ballistically to a point of scattering, after which it reaches the detector without further collisions. In the local approximation of Eqn (5), $\Lambda = L\alpha/4\sin(\alpha/2)$ can be interpreted as the length of the trajectory from the injector to point O (see Fig. 2).

In order to compare the experimental data with theory, it is necessary to extract the contribution of scattered electrons, δV_d^s, from the observed signal δV_d. We have

$$\delta V_d^s = \delta V_d - \exp\left[-\frac{2r_c}{l_{ee}(V_i)}\arcsin\frac{L}{2r_c}\right]\delta V_d^0\,. \tag{7}$$

Here, $\delta V_d^0(B)$ is the signal which would be observed in the absence of scattering, so that the second term on the r.h.s. of Eqn (7) is the contribution of electrons that reach the detector ballistically. Experimentally, $\delta V_d^0(B)$ can be obtained from the experiment at lowest injection energy $V_i = 0.1$ mV. In this case $l_{ee}/L \sim 10^2$ and thus collisions can be neglected. For l_{ee} we use the expression for energy relaxation in a 2DEG obtained by Giuliani and Quinn [2]:

$$l_{ee}(\varepsilon) \approx \frac{4\pi\hbar v}{\varepsilon_F}\left(\frac{\varepsilon_F}{\varepsilon}\right)^2\left[\ln\frac{\varepsilon_F}{\varepsilon} + \frac{1}{2} + \ln\left(\frac{2q_{TF}}{k_F}\right)\right]^{-1}, \tag{8}$$

where q_{TF} is the Thomas – Fermi screening wave vector.

Figure 4a shows the angular distribution functions $g(\alpha)$ for various injector energies obtained from the experimental data in Fig. 2 using Eqns (5), (6), and (7). The various $g(\alpha)$ clearly display the expected small-angle scattering behavior.

For comparison the results of Eqn (9) for various values of V_i are presented together with experimental data for δV_d^s in Fig. 4b. As is evident from the figure, we find a gratifying agreement between theory (markers) and experiment (drawn curves), justifying the assumptions made in extracting $g(\alpha)$ from the experimental data.

For small V_i (Fig. 4, curves corresponding to $V_i = 0.8$ and 1.2 mV) the observed peak width $\delta\alpha$ is only slightly larger than the point contact opening angle Φ. As discussed above, in this limit the experimentally recovered $g(\alpha)$ is smoothed, and we cannot expect to observe the dip at very small angles. The peak in $g(\alpha)$ broadens when the energy of the injected

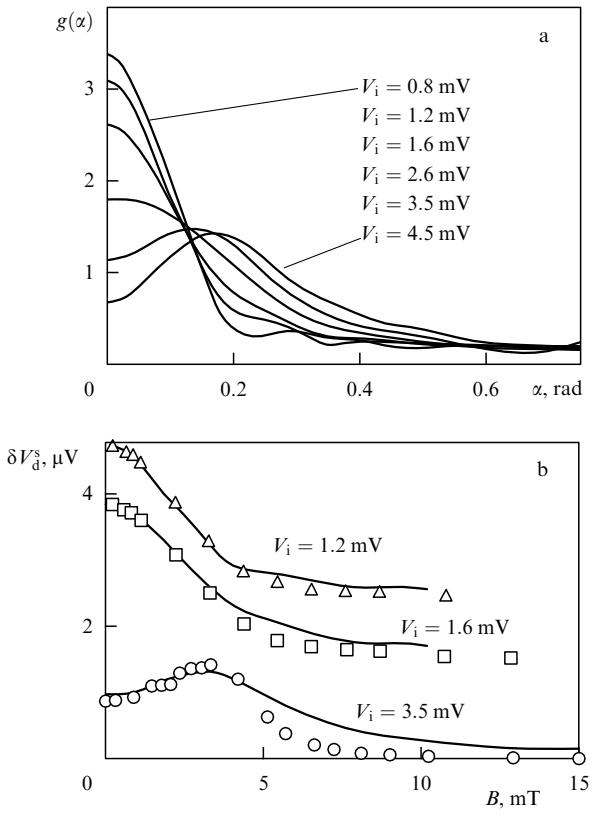

Figure 4. (a) $g(\alpha)$ restored from the experiment. (b) Comparison of the theoretical (markers, Eqn (9)) and experimental (lines, inferred from the experiment using Eqn (7)) δV_d^s. Curves are displaed with an offset for clearness.

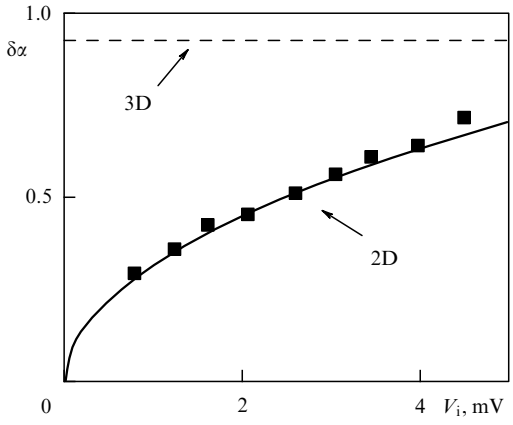

Figure 5. Width $\delta\alpha$ of $g(\alpha)$ (squares) as function of injector bias voltage V_i. $\delta\alpha$ is defined as the angle below which 2/3 of the electrons are scattered. Solid and dashed lines represent theoretical prediction for a 2D ($\delta\alpha \propto (eV_i/E_F)^{1/2}$) and a 3D system, respectively.

electrons is increased ($V_i > 1.5$ mV). In Figure 5 the width of $g(\alpha)$ is displayed as a function of injection energy. It shows a clear square-root behavior $\delta\alpha \propto \sqrt{eV_i/\varepsilon_F}$ in contrast to 3D where g is essentially energy-independent. The increase of $\delta\alpha$ with V_i also directly implies that the small angle scattering observed by us can not be attributed to weak screening in 2D systems. In this case the scattering angle should actually *decrease* with excess energy.

When $\delta\alpha$ becomes larger than the QPC opening angle Φ for higher V_i, one can clearly observe the expected dip in forward direction ($V_i > 3.0$ mV, Fig. 4a). The amplitude of the dip is much larger than would be the case for a 3D electron system.

As discussed above, the local approximation of Eqn (5) is not valid at small scattering angles $\alpha < \Phi$. For these angles, $g(\alpha)$ is more precisely given by the integral equation:

$$\delta V_d^s \simeq 2Cv \int d\varphi \rho_i(\varphi) \int d\varphi' \rho_d(\varphi') \times \tilde{g}\left(\varphi' - \varphi + \frac{L}{r_c}, V_i\right) \kappa\left(\varphi' - \varphi + \frac{L}{r_c}\right), \quad (9)$$

where $\kappa(x) = 1/|x|$ for $x > \Phi$ and $\kappa(x) = 1/\Phi$ for $x < \Phi$. Here again we use $\tilde{g}(\alpha)$ as defined in Eqn (6);

$$\Lambda = L \frac{2\varphi' + L/r_c}{2(\varphi' - \varphi + L/r_c)}$$

is the distance between injector and the crossing point (O) of electron trajectories injected at angle φ and detected at angle φ'; the integration in Eqn (9) has to be evaluated for all Λ such that $0 < \Lambda < L$, while $l_{ee} \equiv l_{ee}(V_i)$.

In conclusion, electron-beam experiments in the 2DEG of GaAs/(Ga,Al)As heterostructures demonstrate unambiguously the occurrence of small-angle ee-scattering characterizing the dimensionality effect on the momentum relaxation in 2D systems. The characteristic scattering distribution function is obtained directly from magnetic-field-dependent beam deflection experiments. The scattering distribution function broadens with increasing electron energy, $\delta\alpha \propto \sqrt{eV_i/\varepsilon_F}$, in contrast to 3D systems where the width is energy-independent. Furthermore, a pronounced dip occurs at small angles. These observations represent conclusive evidence for the manifestation of 2D density-of-states effects in the ee-scattering process.

Acknowledgements. This work was supported in part by Volkswagen Stiftung (Grant I/72531) and by the DFG (MO 771/1–2).

References

1. Chaplik A V *Zh. Eksp. Teor. Fiz.* **60** 1845 (1971) [*Sov. Phys. JETP* **33** 997 (1971)]; Hodges C, Smith H, Wilkins J *Phys. Rev. B* **4** 302 (1971)
2. Guiliani G F, Quinn J J *Phys. Rev. B* **26** 4421 (1982)
3. Gurzhi R N, Kopeliovich A I, Rutkevich S B *Adv. Phys.* **36** 221 (1987); Gurzhi R N, Kalinenko A N, Kopeliovich A I *Phys. Low-Dim. Struct.* (2) 75 (1994)
4. Gurzhi R N, Kalinenko A N, Kopeliovich A I *Phys. Rev. B* **52** 4744 (1995); *Phys. Rev. Lett.* **74** 3872 (1995)
5. Gurzhi R N, Kalinenko A N, Kopeliovich A I *Fiz. Nizk. Temp.* **23** 58 (1997) [*Low Temp. Phys.* **23** 44 (1997)]
6. Laikhtman B *Phys. Rev. B* **45** 1259 (1992)
7. Buhmann H et al. *Fiz. Nizk. Temp.* **24** 978 (1998) [*Low Temp. Phys.* **24** 737 (1998)]
8. Predel H et al. *Phys. Rev. B* **62** 2057 (2000)
9. Molenkamp L W et al. *Phys. Rev. B* **41** 1274 (1990)
10. Sivan U, Heiblum M, Umbach C P *Phys. Rev. Lett.* **63** 992 (1989)
11. Callaway J *Phys. Rev.* **113** 1046 (1959)
12. Cumming D R S, Davies J H *Appl. Phys. Lett.* **69** 3363 (1996)
13. Gurzhi R N, Kalinenko A N, Kopeliovich A I *Surf. Sci.* **361/362** 497 (1996)

Submicron charge-density-wave devices

H S J van der Zant, N Marković, E Slot

Abstract. We review our fabrication methods to produce submicron charge-density-wave (CDW) structures and present measurements of CDW dynamics on a microscopic scale. Our data show that mesoscopic CDW dynamics is different from bulk behavior. We have studied current-conversion and found a size-effect that can not be accounted for by existing models. An explanation might be that the removal and addition of wave fronts becomes correlated in time when probe spacing is reduced below a few μm. On small segments we occasionally observe negative differential resistance in the $I(V)$ characteristics and sometimes the resistance may even become negative. We believe that the interplay between CDW deformations (strain) and quasi-particles may yield non-equilibrium effects that play a crucial role in this new phenomenon. No detailed theoretical calculations are available. Our measurements clearly show the need of a microscopic model for CDW dynamics.

1. Introduction

Electrical conductors with a chain-like structure may exhibit a phase transition to a collective ground state with charge-density waves (CDWs) [1]. The appearance of a CDW state is connected to the Peierls instability [2]: at low temperatures the uniform distribution of conduction electrons of a one-dimensional (1D) conductor is unstable due to their coupling to phonon modes. As a result, the lattice of atoms is distorted and the electrons condense into a ground state with a periodic modulation of the charge density. Collective transport occurs when these CDWs move along the chains. This sliding CDW motion shows similarities with transport in superconductors, with the role of current and voltage reversed. To date, CDW transport has been studied in bulk crystals and has shown many remarkable phenomena. Examples are ac current oscillations induced by a dc electric field and strongly nonlinear electrical properties.

In metallic and superconducting devices, reduction of sizes has revealed a variety of new mesoscopic phenomena. For charge-density-wave (CDW) conductors, the mesoscopic regime has not been studied in detail, largely because samples of (sub)micron sizes could not be fabricated in a controlled way. In this paper, we review our efforts to fabricate small-scale CDW devices of the CDW conductors $NbSe_3$ and o-TaS_3 (Section 2). We discuss two examples of microscopic CDW dynamics in some more detail: a size effect of phase-slip processes in $NbSe_3$ wires (Section 3) and negative resistances in (sub)micron segments of o-TaS_3 (Section 4).

2. Fabrication of mesoscopic CDW structures

We have developed three different techniques for the fabrication of submicron CDW devices. First, we combine an old technique — gluing thin CDW crystals on top of an

H S J van der Zant, N Marković, E Slot Department of Applied Sciences and DIMES, Delft University of Technology, Lorentzweg 1, 2628 CJ Delft, The Netherlands
N Marković Physics Department, Harvard University, 17 Oxford Street, Cambridge, MA 02138 USA